Crack closure, initiation and damage stresses of Montney shale

Qiang Chen and Ron Wong
Department of Civil Engineering, Schulich School of Engineering, University of Calgary, T2N 1N4, Calgary, AB, Canada

ABSTRACT
The uniaxial and triaxial compression tests have been conducted on 38 mm diameter core plugs to characterize the mechanical properties of the Montney strata. The crack closure, crack initiation, crack damage and peak stresses are determined based on the test results. The axial strain response method (ASRM), the lateral strain response method (LSRM), the volumetric strain method (VSM) and the crack volumetric strain method (CVSM) are used to estimate these 4 stress thresholds. The results show that all methods can give acceptable values. ASRM and LSRM depend heavily on the origin of the stress-strain curve. In addition, the Young's modulus, Poisson's ratio, cohesion and friction angle are obtained from the test results.

RÉSUMÉ
Les essais de compression uniaxiale et triaxiale ont été effectués sur des bouchons de 38 mm de diamètre afin de caractériser les propriétés mécaniques des strates de Montney. La fermeture, l'amorçage et le dommage des fissures et les pics de contrainte sont déterminés en fonction des résultats des essais. Les méthodes de réponse en déformation axiale (ASRM)et latérale (LSRM), et les méthodes de déformation volumétrique (VSM) et volumétrique de fissure (CVSM) sont utilisées pour estimer ces 4 seuils de contrainte. Les résultats montrent que toutes les méthodes peuvent donner des valeurs acceptables. L'ASRM et le LSRM dépendent fortement de l'origine de la courbe contrainte-déformation. De plus, le module de Young, le coefficient de Poisson, la cohésion et l'angle de frottement sont obtenus à partir des résultats des essais.

1 INTRODUCTION

The Montney Formation is a Lower Triassic stratum covering approximately 130,000 km^2 in British Columbia and Alberta (Alberta Energy Regulator, 2013; Rivard et al., 2014). Because the permeability of the tight shale is very low (NEB, 2009), horizontal drilling and multi-stage hydraulic fracturing are indispensable for the development of this unconventional reservoir (Alberta Energy Regulator, 2013). However, potential risks to water resources and induced seismic events associated with hydraulic fracturing have arisen intense public concerns (Bao and Eaton, 2016; Vengosh et al., 2014). Significant efforts have been made to improve the prediction of the resulting geometry of the hydraulic fractures (Economides and Nolte, 2000). Basic geomechanical properties of Montney shale like Young's modulus and Poisson's ratio are usually needed in the design and modelling of hydraulic fracturing.

In this paper, two uniaxial compression and three triaxial compression tests have been done on Montney core plugs to characterize the deformation and strength properties of the Montney strata because of the limited number of samples available The Young's modulus and Poisson's ratio were calculated. The strength data were fitted using the Mohr-Coulomb and Hoek-Brown strength criteria. In addition, the crack closure stress σ_{cc}, crack initiation stress σ_{ci}, and crack damage stress σ_{cd} were evaluated using various methods including the volumetric strain method (VSM), the crack volumetric strain method (CVSM), the lateral strain response method (LSRM) and the axial strain response method (ASRM).

2 DEFORMATION AND FRACTURE OF BRITTLE ROCK

Many researchers have investigated the failure of brittle rocks (Bieniawski, 1967; Brace, 1964; Brace et al., 1966; Martin and Chandler, 1994; Eberhardt et al., 1998; Diederichs, 2000; Ghazvinian, 2010). The results show that the pre-peak part of the brittle failure of rocks can be divided into four stages as shown in Figure 1, based on the stress-strain curve:

(I) Closure of existing microcracks
(II) Linear elastic deformation
(III) Crack initiation and stable crack growth
(IV) Crack damage and unstable crack growth

From low to high, the stress thresholds separating the stages are the crack closure stress σ_{cc}, crack initiation stress σ_{ci}, crack damage stress σ_{cd} and peak stress σ_c.

In the crack closure stage, the pre-existing cracks will gradually close and the stiffness of the sample increases with the loading. The extent of this stage depends on the initial crack density and crack geometry (Stage I). Once most of the cracks have closed, the sample becomes a linear elastic material. The Young's modulus and Poisson's ratiocan be determined from this stage (Stage II) (Martin and Chandler, 1994).

The onset of the crack growth marks the beginning of Stage III. It is this stress level where dilatancy starts (Brace et al., 1966). The crack propagation in this stage is considered stable which means the crack propagation ceases once the load stops. According to Bieniawski (1967), the fracture propagation is stable only if there exists

a definite relationship between the crack length and the applied stress.

The reversal of the total volumetric strain marks the beginning of unstable crack growth (Stage IV). The governing factor in the unstable fracture propagation is the crack velocity (Bieniawski, 1967). The relationship between the axial stress and axial strain becomes nonlinear, which indicates relative sliding along flaws and grain boundaries.

The peak strength of the material marks the beginning of post-peak behaviour. During the first portion of the post-peak stress descent, the loci of the seismic events indicate the development of a major inclined shear fracture (Lockner et al., 1991).

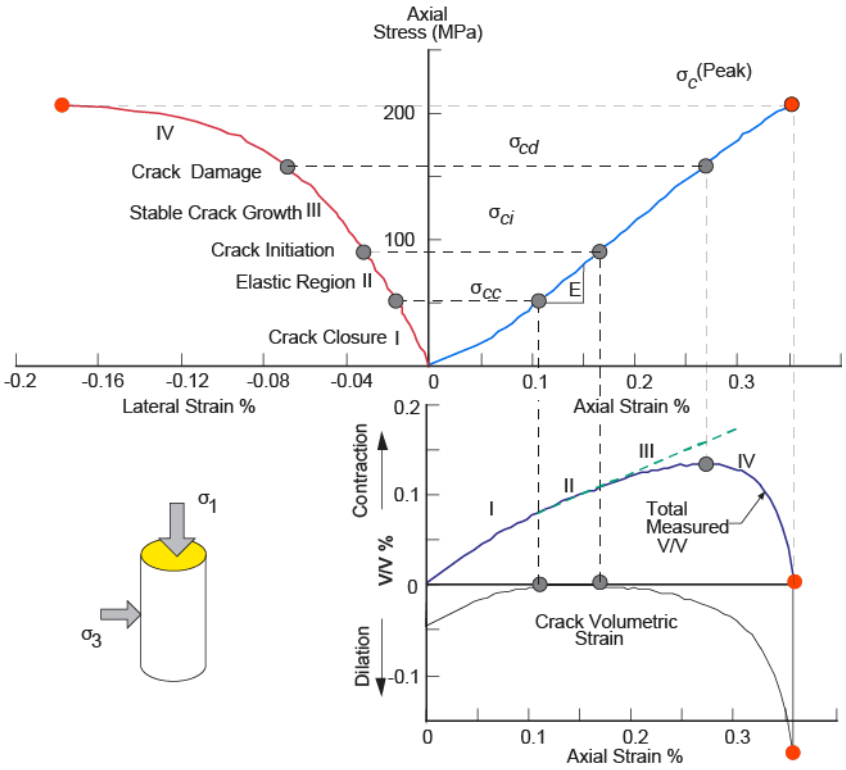

Figure 1. Stress-strain curve showing the four stages in rock failure process (after Cai, 2010)

2.1 Determination of Each Stress Level

The two most common methods for detecting the stress levels are the acoustic emission method and the strain measurement method (Eberhardt et al., 1998). Ghazvinian (2010) suggested that the acoustic emission method could give more accurate the stress levels after comparing these two methods. However, the instruments required for monitoring the acoustic emission events are not available in our lab. Thus, only the strain measurement method will be used. The crack damage stress σ_{cd} is calculated as the axial stress where the total volumetric strain reverses (Bieniawski, 1967).

2.1.1 Methods Based on Volumetric Strain

2.1.1.1 Volumetric Strain Method (VSM)

The volumetric strain method was first proposed by Brace et al. (1966) during the investigation of volume change of rock under confining pressure. It can be used to estimate the crack closure stress σ_{cc} and crack initiation stress σ_{ci}. σ_{cc} is determined as the axial stress where the axial stress-volumetric strain curve starts to be linear. σ_{ci} is the stress level where the linear portion ends.

2.1.1.2 Crack Volumetric Strain Method (CSVM)

The crack volumetric strain method was introduced by Martin and Chandler (1994) because it is difficult to identify σ_{ci} from the stress-strain curve especially for samples with a high density of cracks. The crack volumetric strain ε_{cv} is the difference between the total volumetric strain ε_v and the elastic volumetric strain ε_e.

$$\varepsilon_{cv} = \varepsilon_v - \varepsilon_e \quad [1]$$

The volumetric strain ε_v can be calculated using the axial stain ε_1 and radial strain ε_3

$$\varepsilon_v = \varepsilon_1 + 2\varepsilon_3 \quad [2]$$

The elastic volumetric strain can be determined based on the linear elastic constants (E, ν) from the linear elastic stage.

$$\varepsilon_e = \frac{1-2\nu}{E}(\sigma_1 - \sigma_3) \quad [3]$$

There exists a horizontal line in the plot of crack volume strain versus axial strain (Figure 1). The stress at which the horizontal line starts is σ_{cc}. The stress at which the horizontal line ends is σ_{ci}.

2.1.2 Methods Based on Axial and Lateral Strain

2.1.2.1 Lateral Strain Response Method (LSRM)

Bieniawski (1967) and Lajtai (1974) proposed that the crack initiation stress can be determined as the point where the lateral strain curve departs from linearity. Stacey (1981) takes the point at which the plot of lateral strain versus axial strain starts to become nonlinear as the crack initiation stress. Nicksiar and Martin (2012) proposed the lateral strain response method (LSRM) to determine the crack initiation stress. In this method, a reference line, which connects the damage stress point and the origin on the axial stress versus lateral strain plot, is required. The point corresponding to the maximum difference between the lateral stain and the reference line is the crack initiation stress σ_{ci}.

2.1.2.2 Axial Strain Response Method (ASRM)

Using similar approach as the LSRM, Peng et al. (2015) proposed the axial strain response method (ASRM) to identify the crack closure stress. The crack closure stress σ_{cc} is the stress corresponding to the maximum difference between the axial strain and the reference line, which connects the damage stress and the origin on the stress versus axial strain plot.

3 SAMPLES AND TESTING APPARATUS

3.1. Material Used

The details on the sample ID and depth are given in Table 1. Samples 2V1, 2V2, 2V3 and 2V5 were cored using water as the drilling fluid. Sample 7G2-2 was cored using nitrogen gas as the drilling fluid. They were all 38 mm in diameter and the length to diameter ratio was around 2.

Table 1. Locations of the samples

ID	Depth m
7G2-2	3037.65
2V5	3046.55
2V1	3046.65
2V2	3046.80
2V3	3046.90

3.1 Testing Apparatus

For sample 2V1, it was tested with the GCTS testing system and the confining pressure was 20 MPa. Two axial LVDT and 1 radial LVDT were used to measure the axial and radial displacements, respectively.

The other tests were done with a 2.2 MN MTS load frame (Model 311.41.360). Four strain gauges (2 horizontal and 2 vertical) were used to measure the strains. The strain gauges were about 10 mm in length and 3.5 mm in width, with a resistance of 120.0 ± 0.15% Ohms and gauges factor of 2.135 ± 0.15%. The setup for UCS test is shown in Figure 2. The cell used for confined tests is the Hoek cell suitable for 38-mm diameter samples (Figure 3).

Figure 2. Setup for uniaxial compression test (2.2 MN load frame in the University of Calgary lab)

Figure 3. Hoek cell setup

4 TEST RESULTS

The stress-strain curves of the 5 tests are given in the appendix. The pictures of the samples after tests are given in Figure 4.

Figure 4. Samples after test (samples 7G2-2, 2V1, 2V2, 2V3)

For the UCS tests, the samples failed in an explosive fashion, broke into pieces and some of the pieces flew several meters away from the load frame. Most of the fractures are parallel to the maximum stress direction. For the triaxial compression tests, there are always one inclined dominating fracture. The fracture angle is very steep. With increasing confining pressure (2V2, 2V1, 2V3), the fracture angle decreases.

4.1 Young's Modulus, Poisson's Ratio and Strength Envelope

The Young's modulus, E, and Poisson's ratio, ν, were determined using least square method based on manually selected linear portion of the primary stress-strain curve (see appendix). The strength, σ_c, is the maximum deviatoric stress achieved. The results are given in Table 2. Engineering stress and strain were used in the calculation.

Table 2. E, ν and σ_c of the compression test results

ID	σ_3 MPa	E GPa	ν	σ_c MPa
7G2-2	0	56.7	0.21	203.8
2V5	0	37.0	0.25	161.5
2V1	20	49.9	0.36	376.4
2V2	10	37.3	0.24	318.2
2V3	40	43.2	0.23	446.3

Based on the results of samples 2V2, 2V1, 2V3, 2V5, the Mohr-Coulomb and Hoek-Brown strength criteria were employed to curve fit the data (Figure 5). For the details of the fitting methods, please refer to You (2011). The fitting result using Coulomb criterion is (unit in MPa):

$$\sigma_1 = 210.2 + 7.6\sigma_3 \quad [4]$$

The tensile strength is predicted to be -27.7 MPa. The cohesion is 38.1 MPa and the friction angle is 50.1°

The fitting result using Hoek-Brown criterion is (unit in MPa):

$$\sigma_1 = \sigma_3 + 182.5\sqrt{26\frac{\sigma_3}{182.5}+1} \quad [5]$$

The tensile strength is predicted to be -7.0 MPa

4.2 Crack Closure, Initiation and Crack Damage Stresses

One radial strain gauge connecting to sample 2V5 was not working properly during the last stage of test. Thus, the crack closure, initiation and damage stresses were not determined for this sample.

The crack closure stress values were determined for samples 7G2-2, 2V2, 2V1 and 2V3 using the methods described in Section 2.1. The results are given in Table 3. The crack initiation stress values of the four samples were also determined and given in Table 4. The details about the determination procedure of sample 7G2-2 are shown in the appendix. In addition, the mean value, standard deviation (SD) and coefficient of variation (CoV) were also provided. The values in red are abnormal results. The reason is that ASRM and LSRM depend heavily on the origin of the stress-strain curve. However, the accuracy of the origin is usually low due to seating effect as shown in the stress-strain curve of sample 2V1 (given in the appendix).

Table 3. Estimation results of crack closure stress

ID	Crack closure stress σ_{cc} (MPa)						σ_{cd} (MPa)	σ_c (MPa)	σ_{cd}/σ_c	σ_{cc}/σ_{cd}	σ_{cc}/σ_c
	VSM	CVSM	ASRM	Mean	SD	CoV (%)					
7G2-2	54.4	51.8	47.1	51.1	3.0	5.9	175.2	203.8	0.86	0.292	0.251
2V2	73.3	74.9	66.8	71.7	3.5	4.9	213.1	318.2	0.67	0.336	0.225
2V1	100.9	119.2	162.8	110.1	9.2	8.3	307.8	376.4	0.82	0.358	0.292
2V3	109.0	99.8	86.1	104.4	4.6	4.4	339.7	446.3	0.76	0.307	0.234

Table 4. Estimation result of crack initiation stress

ID	Crack initiation Stress (MPa)						σ_{cd} (MPa)	σ_c (MPa)	σ_{cd}/σ_c	σ_{ci}/σ_{cd}	σ_{ci}/σ_c
	VSM	CVSM	LSRM	Mean	SD	CoV (%)					
7G2-2	103.3	105.3	101.8	103.5	1.4	1.4	175.2	203.8	0.86	0.591	0.508
2V2	134.1	136.6	118.8	129.8	7.9	6.1	213.1	318.2	0.67	0.609	0.408
2V1	161.8	181.4	110.3	171.6	9.8	5.7	307.8	376.4	0.82	0.558	0.456
2V3	209.4	205.9	206.1	207.1	1.6	0.8	339.7	446.3	0.76	0.610	0.464

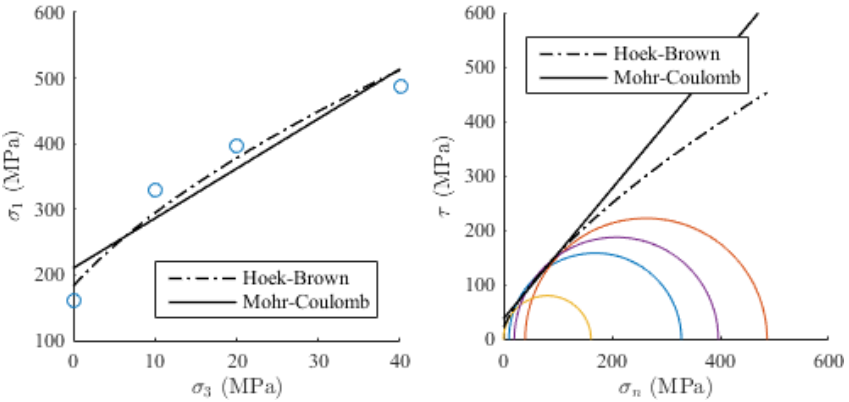

Figure 5. Mohr-Coulomb and Hoek-Brown envelopes (the UCS of sample 7G2-2 is not included because it is not in the same depth interval as the other samples)

It is found that σ_{cd}/σ_c ranges from 0.67 to 0.86, which is consistent with the result by Martin and Chandler (1994). Both σ_{cc} and σ_{ci} increase with the confining pressure. However, the values of σ_{cd}/σ_c , σ_{cc}/σ_{cd} , σ_{cc}/σ_c , σ_{ci}/σ_{cd}, σ_{ci}/σ_c are insensitive to confining pressure.

5 DISCUSSION

Multi-stage triaxial tests have been done on 38 mm diameter Montney core plugs from the same well by McKean (2017). The confining pressures for the multi-stage triaxial tests were 15, 30, 45 and 60 MPa. The results of two vertical samples (depths of 3141.75 m and 3149.82 m) will be introduced here. For the sample 3141.75(V), the cohesion and friction angle of the Mohr-Coulomb failure criterion are 63.7 MPa and 42° while the UCS and parameter m of the Hoek-Brown criterion are 252 MPa and 14.1. For the sample 3149.82(V), the cohesion and friction angle of the Mohr-Coulomb failure criterion are 59.6 MPa and 36.5° while the UCS and m of the Hoek-Brown criterion are 216 MPa and 9.3. The effect of confining pressure on the strength observed by McKean (2017) is much lower than that observed in this study. The reason might be that the damage from the previous stages will reduce the rock strength for the next stages in a multi-stage triaxial test.

The ASRM and LSRM can give results which are consistent with the volumetric strain method (VSM) and crack volumetric strain method (CVSM). However, if the seating effect of the sample is notable like sample 2V1, these two methods will not give the correct value.

6 CONCLUSION

Two uniaxial compression and three triaxial compression tests have been done on Montney core plugs and their basic geomechanical properties were determined in this paper. The Young's modulus values range from 36.9 GPa to 56.9 GPa and the Poisson's ratios have a range from 0.21 to 0.39. According to Mohr-Coulomb criterion, the cohesion is 38.1 MPa and the friction angle is 50.1°. The parameters for Hoek-Brown criterion are $\sigma_{ucs} = 182.5$ MPa and $m = 26$.

σ_{cd}/σ_c ranges from 0.67 to 0.86. Both σ_{cc} and σ_{ci} increase with the confining pressure. However, the values of σ_{cd}/σ_c, σ_{cc}/σ_{cd}, σ_{cc}/σ_c, σ_{ci}/σ_{cd}, σ_{ci}/σ_c are insensitive to confining pressure.

The ASRM and LSRM all give results which are consistent with that obtained from the volumetric strain method and crack volumetric strain method. ASRM and LSRM depend heavily on the origin of the stress-strain curve.

7 ACKNOWLEDGEMENT

The authors wish to acknowledge the funding provided by Seven Generations Energy Ltd. and the Department of Civil Engineering at the University of Calgary. The samples

were provided by Seven Generations Energy Ltd. Technical assistance provided by Mirsad Berbic and Donald Anson during tests is greatly appreciated.

8 REFERENCES

Alberta Energy Regulator. 2013. *Energy Briefing Note: The Ultimate Potential for Unconventional Petroleum from the Montney Formation of British Columbia and Alberta*. Alberta Energy Regulator, AER/AGS Information Series 144.

Bao, X., Eaton, D.W., 2016. Fault Activation by Hydraulic Fracturing in Western Canada. *Science,* 354:1406–1409.

Bieniawski, Z.T. 1967. Mechanism of Brittle Fracture of Rock: Part I—Theory of the Fracture Process. *International Journal of Rock Mechanics and Mining Sciences & Geomechanics Abstracts,* 4:395–406.

Brace, W. F. 1964. Brittle Fracture of Rocks, in: Judd, W.R. (Ed.), *State of Stress in the Earth's Crust*. Elsevier, Santa Monica, USA, pp. 111–174.

Brace, W.F., Paulding, B.W., Scholz, C.H. 1966. Dilatancy in the Fracture of Crystalline Rocks. *Journal of Geophysical Research,* 71:3939–3953.

Cai, M. 2010. Practical Estimates of Tensile Strength and Hoek-Brown Strength Parameter m of Brittle Rocks. *Rock Mechanics and Rock Engineering*, 43:167–184.

Diederichs, M. S. 2000. Instability of hard rockmasses, the role of tensile damage and relaxation. PhD thesis, University of Waterloo, Waterloo, Ontario, Canada.

Eberhardt, E., Stead, D., Stimpson, B., Read, R. S. 1998. Identifying crack initiation and propagation thresholds in brittle rock. *Canadian Geotechnical Journal*, 35(2):222-333.

Economides, M. J., Nolte, K. G. 2000. *Reservoir Stimulation*, 3rd ed. John Wiley & Sons Ltd.

Ghazvinian, E. 2010. Modelling and testing strategies for brittle fracture simulation in crystalline rock samples. MSc thesis, Queen's University, Kingston, Ontario, Canada.

Lajtai, E.Z. 1974. Brittle Fracture in Compression. *International Journal of Fracture*, 10:525–536.

Lockner, D.A., Byerlee, J.D., Kuksenko, V., Ponomarev, A., Sidorin, A. 1991. Quasi-Static Fault Growth and Shear Fracture Energy in Granite. *Nature*, 350:39–42.

Martin, C.D., Chandler, N.A. 1994. The Progressive Fracture of Lac du Bonnet Granite*. International Journal of Rock Mechanics and Mining Sciences & Geomechanics Abstracts*, 31:643–659.

McKean, S.H. 2017. Geomechanical Properties of the Montney and Sulphur Mountain Formations. MSc thesis. University of Calgary, Calgary, Alberta, Canada.

NEB, 2009. *A Primer for Understanding Canadian Shale Gas - Energy Briefing Note, National Energy Board of Canada*. National Energy Board of Canada.

Nicksiar, M., Martin, C.D. 2012. Evaluation of Methods for Determining Crack Initiation in Compression Tests on Low-Porosity Rocks. *Rock Mechanics and Rock Engineering*, 45:607–617.

Peng, J., Cai, M., Rong, G., Zhou, C.-B., Zhao, X. 2015. Stresses for Crack Closure and its Application to Assessing Stress-Induced Microcrack Damage. *Chinese Journal of Rock Mechanics and Engineering*, 6:1091–1100.

Rivard, C., Lavoie, D., Lefebvre, R., Séjourné, S., Lamontagne, C., Duchesne, M., 2014. An Overview of Canadian Shale Gas Production and Environmental Concerns. *International Journal of Coal Geology*, 126:64–76.

Stacey, T.R. 1981. A Simple Extension Strain Criterion for Fracture of Brittle Rock. *International Journal of Rock Mechanics and Mining Sciences*, 18:469–474.

Vengosh, A., Jackson, R.B., Warner, N., Darrah, T.H., Kondash, A. 2014. A Critical Review of the Risks to Water Resources from Unconventional Shale Gas Development and Hydraulic Fracturing in the United States. *Environmental Science & Technology*, 48:8334–8348.

You, M. 2011. Comparison of the Accuracy of Some Conventional Triaxial Strength Criteria for Intact Rock. *International Journal of Rock Mechanics and Mining Sciences*, 48:852–863.

APPENDIX

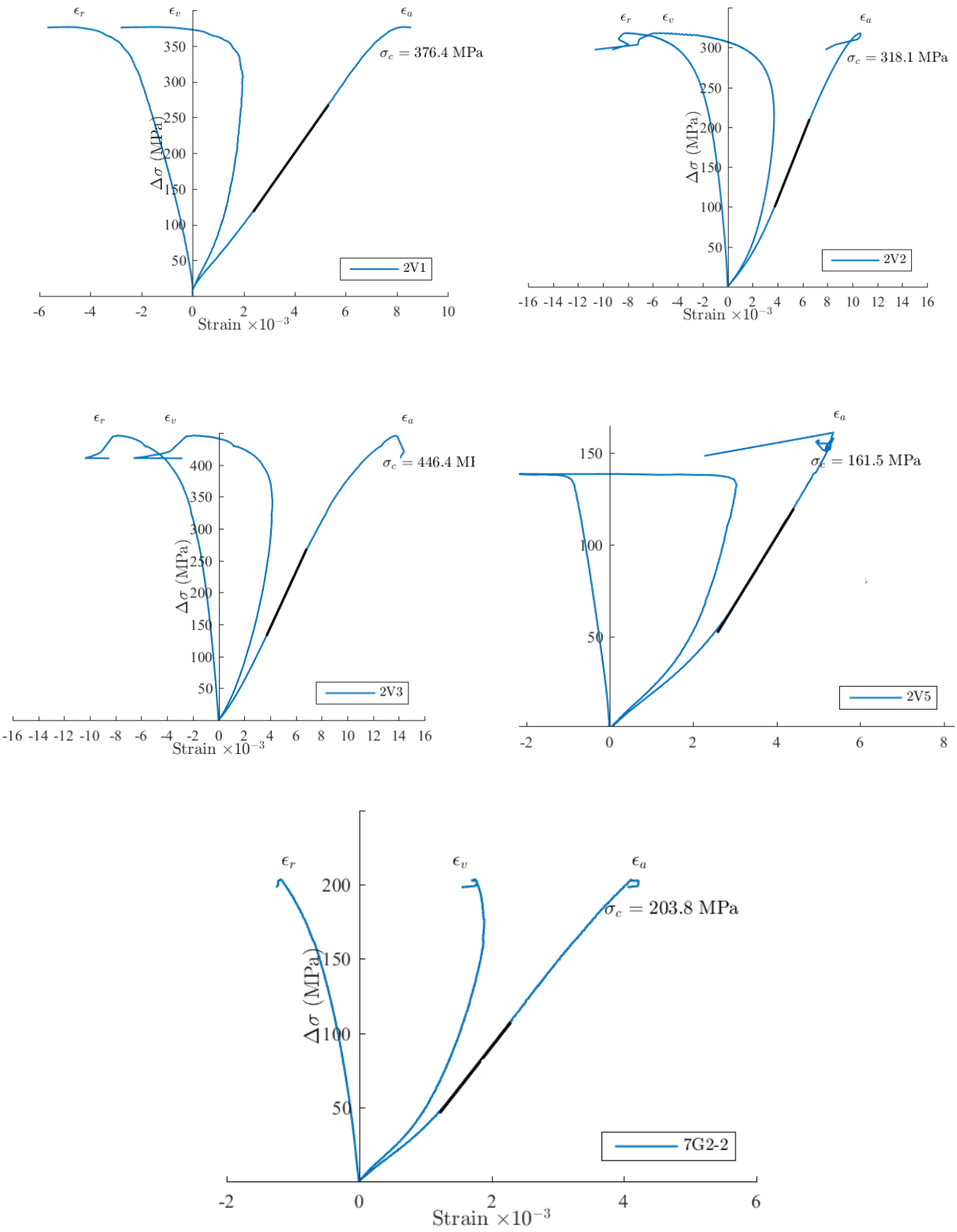

Figure 6. Stress-strain curves of samples 2V1, 2V2, 2V3 2V5 and 7G2-2

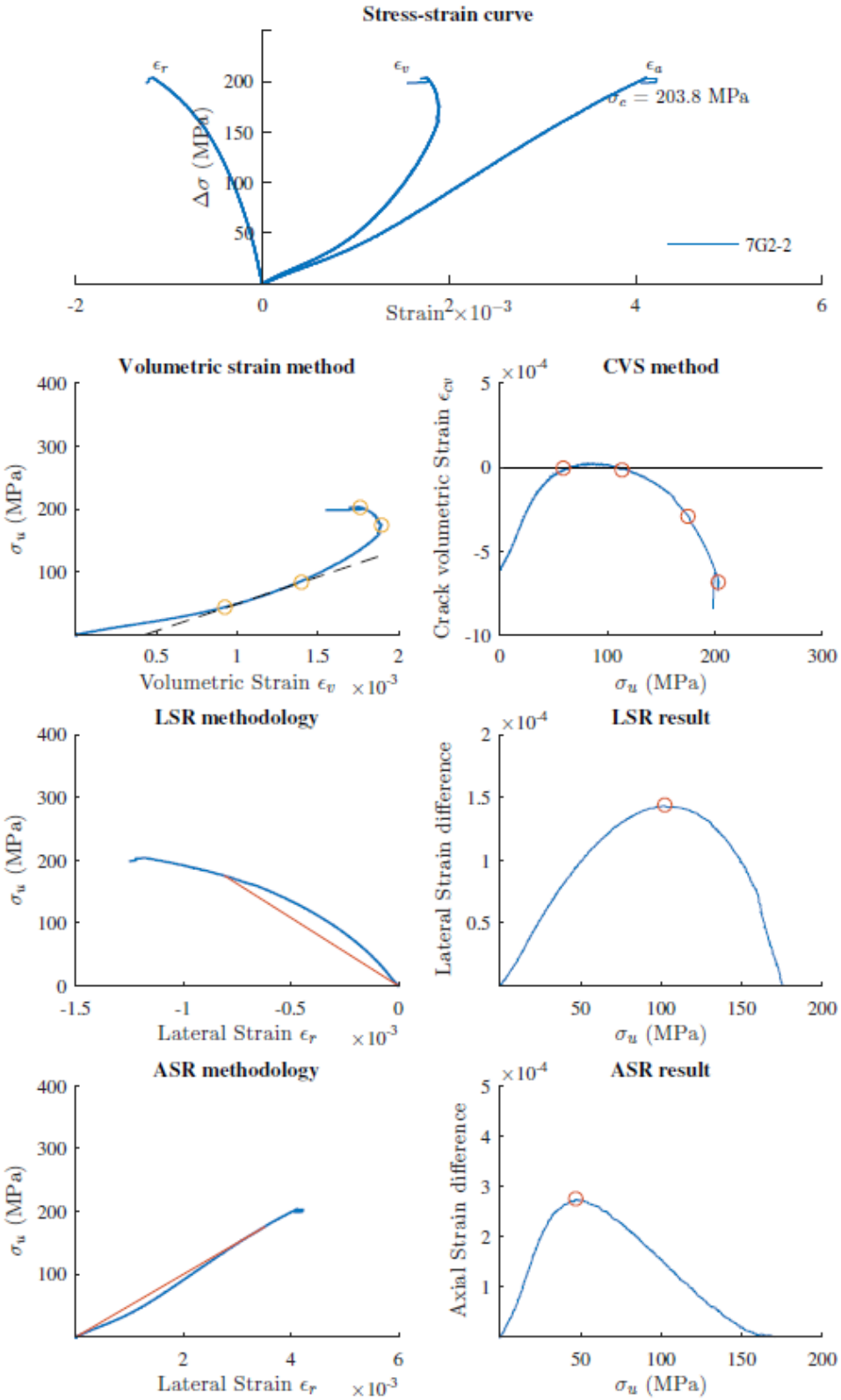

Figure 7. Estimation of crack closure, initiation and damage stresses of sample 7G2-2